X-ray photoelectron spectra structure and chemical bond nature in NpO_2

Yu. A. Teterin,* A. Yu. Teterin, and K. E. Ivanov
NRC "Kurchatov Institute", Moscow, 123182, Russia

M. V. Ryzhkov
Ural Department of RAS, Institute of Solid State Chemistry, Ekaterinburg, 620990, Russia

K. I. Maslakov, St. N. Kalmykov, V. G. Petrov, and D. A. Enina
Chemistry Department, Lomonosov Moscow State University, Moscow, 119991, Russia

(Received 1 October 2013; published 3 January 2014)

Quantitative analysis was done of the x-ray photoelectron spectra structure in the binding energy (BE) range of 0 to ∼35 eV for neptunium dioxide (NpO_2) valence electrons. The BEs and structure of the core electronic shells (∼35–1250 eV) as well as the relativistic discrete variation calculation results for the finite fragment of the NpO_2 lattice and the data of other authors were taken into account. The experimental data show that the many-body effects and the multiplet splitting contribute to the spectral structure much less than the effects of formation of the outer (0–∼15 eV) and the inner (∼15–∼35 eV) valence molecular orbitals (OVMO and IVMO, respectively). The filled Np 5f electronic states were shown to form in the NpO_2 valence band. The Np 6p electrons participate in formation of both the IVMO and the OVMO (bands). The filled Np $6p_{3/2}$ and the O 2s electronic shells were found to take the maximum part in the IVMO formation. The MO composition and the sequence order in the BE range 0–∼35 eV in NpO_2 were established. The experimental and theoretical data allowed a quantitative MO scheme for NpO_2, which is fundamental for both understanding the chemical bond nature in neptunium dioxide and the interpretation of other x-ray spectra of NpO_2.

DOI: 10.1103/PhysRevB.89.035102 PACS number(s): 73.20.At

I. INTRODUCTION

The study of neptunium electronic structure and the chemical bonding nature in neptunium oxides is a topic of great interest in experimental[1–8] and theoretical[9–20] studies since neptunium is a technologically important actinide accumulated in high-level radioactive wastes during a regular nuclear fuel cycle.[1,2,4]

When doing the x-ray photoelectron spectroscopy (XPS) study of lanthanide,[21,22] actinide,[21,23] and other[21] compounds, a structure was found not only in the 0 to ∼15 eV binding energy (BE) range, but also in the ∼15 to ∼35 eV range. The observed peaks were found to be several electron volts wide, which sometimes is wider than the corresponding core electron peaks.

One of the reasons established for such an XPS structure formation was the formation of the outer valence molecular orbitals (OVMO; 0 to ∼15 eV BE) and the inner valence molecular orbitals (IVMO; ∼15 to ∼35 eV BE), with a significant participation of the filled Ln 5p and the An 6p atomic shells of lanthanides and actinides and the neighboring e.g. O 2s atomic shells of oxygen.[21–23] Practically, these spectra reflect the valence band (0–∼35 eV) structure and are observed as several electron-volts-wide lines. Under certain conditions, the IVMOs were shown to be able to form in compounds of any elements of the periodic table.[21]

Previously, the XPS were measured in the 0–1000 eV BE range from a NpO_2 thin film on Pt surface,[2,3,4] the Np 4f XPS—from polycrystalline NpO_2,[4–6] and from Np and an oxide film formed on a metallic Np surface.[7,8] The photoelectron spectra at 21.2 eV (HeI), 40.8 eV (HeII), and 48.4 eV (HeII*) excitation energies from polycrystalline neptunium oxides,[4] and neptunium oxides formed on a metallic neptunium surface, were measured as well.[8] The electronic structure calculation in the 0–∼35 eV BE range in the nonrelativistic cluster approximation of the X_α-discrete variation method was also done.[10] It allowed only a qualitative interpretation of the ∼15–∼35 eV BE XPS structure from NpO_2. The calculation results for the 0–∼15 eV BE range[9,11–20] also allowed a qualitative valence XPS interpretation. The XPS studies of metallic Np[5,7,9] and oxides NpO_x on the metal surface[5–8] were focused mostly in the OVMO and the Np 4f BE ranges. However, the structure of the inner valence and the core levels of NpO_2 were practically not studied.[2,3] The valence XPS structure in the 0–∼35 eV BE range was studied, e.g. for ThO_2,[24] UO_2,[25] PuO_2,[26] γ-UO_3,[27] UF_4,[28] and UO_2F_2.[29]

This paper analyzes the XPS from NpO_2 films on Pt surface and polycrystalline NpO_2 powder in the BE range 0–1250 eV and quantitatively interprets the XPS structure in the BE range 0–∼35 eV, taking into account the photoelectron[4,5,8] and the x-ray photoelectron[2–4] spectroscopy BEs and core electron spectral structure parameters, as well as the self-consisting field relativistic discrete variation (SCF RDV) calculation results for the NpO_8 (D_{4h}) cluster reflecting Np close environment in NpO_2.

II. EXPERIMENTAL

A. Samples

1. NpO_2 synthesis from oxalate

The standard nitrate ^{237}Np solution, deionized water, and chemically pure reagents were used for the sample preparation.

Oxalic acid in abundance was added to nitric ^{237}Np(IV) solution and thoroughly mixed. The precipitate was separated by centrifugation and washed three times in ethanol. Several drops

of water were added to the obtained $Np(C_2O_4)_2$ precipitate, and the suspension was gradually put on the platinum substrate. Afterwards, the sample on the substrate was left under a 500-W lamp to dry. Then the sample was annealed in a muffle furnace according to the following program: 20 h heating to 700 °C; 5 h heating from 700 to 1200 °C; 10 h annealing at 1200 °C; and 15 h cooling from 1200 °C to room temperature. Tetravalent neptunium oxalate decomposition reaction is seen in Eq. (1):

$$Np(C_2O_4)_2 \xrightarrow{t^\circ} NpO_2 + 2CO_2\uparrow + 2CO\uparrow. \quad (1)$$

2. *Electrolytic synthesis of NpO_2*

A nitric neptunium solution of $\sim 10^{19}$ atoms was placed in the electrolytic cell with platinum substrate as a cathode. Platinum wire was used as an anode; ammonium nitrate NH_4NO_3 was used as an electrolyte. The process was carried out at 1 A and 30 mV for 1–2 h until neptunium was extracted completely from the solution. Aliquots of 20 μl were taken periodically to control the neptunium contents in the solution by liquid scintillation spectrometry. After the electrolysis was completed, the sample on the substrate was placed in a muffle furnace and annealed by the same program as it was done for oxalate decomposition.

3. *Sample preparation for XPS measurements*

NpO_2 samples were prepared as dense thick layers on a platinum substrate (Ø14-mm foil). Neptunium dioxide surface was Ø 4–5 mm. The finely dispersed NpO_2 sample was prepared by the oxalate technique. The most repeatable and reliable data were obtained from the powder samples as thick dense layers with a flat surface on the two-sided conducting adhesive tape. The samples by these techniques were prepared three times in order to obtain the repeatable results. NpO_2 as well as impurities formation on the sample surface were controlled by the XPS in the BE range 0–1250 eV. The Np 4f, the O 1s, and the low-BE XPS structure in this case is more representational. Sample surface Ar^+ etching at 2.5 keV and 10 μA during the periods of time from 10 s to 3 min was done. The XPS studies of the sample surface after 1 d and 1 mo in the air were also done.

B. X-ray photoelectron measurements

X-ray photoelectron spectra of NpO_2 were measured with an electrostatic spectrometer Quantera Scanning XPS Microprobe (Quantera SXM) using monochromatized $AlK_{\alpha 1,2}$ ($h\nu = 1486.6$ eV) radiation (Ø50-μm beam) under 1.3×10^{-7} Pa at room temperature. The device resolution measured as the full width on the half-maximum (FWHM) of the Au 4$f_{7/2}$ peak was 0.7 eV. The binding energies E_b (eV) were measured relative to the BE of the C 1s electrons from hydrocarbons absorbed on the sample surface that was accepted to be equal to 285.0 eV. The FWHMs are given relative to that of the C 1s XPS peak from hydrocarbon on the sample surface being 1.3 eV.[22] The error in the determination of the BE and the peak widths did not exceed ±0.1 eV, and the error of the relative peak intensity ±10%. The inelastically scattered electrons-related background was subtracted with the Shirley method.[30]

The quantitative elemental analysis of several nanometer-deep layers of the studied samples was done. It was based on the fact that the spectral intensity is proportional to the number of certain atoms in the studied sample. The following ratio was used: $n_i/n_j = (S_i/S_j)(k_j/k_i)$, where n_i/n_j is the relative concentration of the studied atoms, S_i/S_j is the relative core-shell spectral intensity, and k_j/k_i is the relative experimental sensitivity coefficient. The following coefficients relative to the C 1s were used: 0.25 (C 1s); 0.70 (O 1s); 9.6 (Np 4$f_{7/2}$; see, e.g. Refs. 31 and 32). The best stoichiometric composition of neptunium dioxide was $NpO_{1.95}$, taking into account the O 1s and the Np 4$f_{7/2}$ peaks, which within the error agrees with NpO_2.

III. CALCULATIONS

The electronic structure calculations were made for the fragment of crystal lattice (NpO_8 cluster). The cluster reflecting Np close environment in NpO_2 is a body-centered cube with Np in the center and eight oxygens in the corners. The Np-O interatomic distance is $R_{Np\text{-}O} = 0.2354$ nm.[33] In this paper, the electronic structure is calculated in the density functional theory (DFT) approximation using the original code of the fully RDV cluster method[34,35] with exchange-correlation potential.[36] The RDV method is based on the solution of the Dirac-Slater equation for the 4-component wave functions transforming according to the irreducible representations of the double point group (D_{4h}; in the present calculations). For the calculation of symmetry coefficients, we used the original code, which realizes the projection operators' technique[34] and includes the matrices of the irreducible representations of the double point groups[37] and the transformation matrices presented in Ref. 38. The extended basis of the 4-component numerical atomic orbitals (AOs) obtained as the solution of the Dirac-Slater equation for isolated neutral atoms also included the Pu 7$p_{1/2}$ and the Pu 7$p_{3/2}$ functions in addition to the occupied AOs. The use of such "most natural basis orbitals" and the absence of any muffin-tin (M-T) approximation to potential and electronic density allow one to describe the formation of interatomic bonds; in such an approach, this description is more illustrative than that obtained in the band structure approach. Numerical diophantine integration in matrix elements calculations was carried out for 22 000 (NpO_8) sample points distributed in the cluster space. It provided the convergence of MO energies better than 0.1 eV. Since a cluster is a fragment of a crystal, the renormalization of the valence ligand AO population was done during the self-consistent field calculations. It allowed an effective consideration of the stoichiometry of the compound and the charge redistribution between oxygens and the ambient crystal.

IV. RESULTS AND DISCUSSION

The XPS identification of Np on the sample surface beside the traditional XPS parameters [chemical shifts (ΔE_b) and peak intensities (I_0)] can employ the core and valence spectral structure parameters in the BE range 0–1250 eV.[23] These XPS structure parameters are typical for neptunium dioxide and work like "fingerprints". In this paper, the XPS from the samples prepared by different techniques were identical within

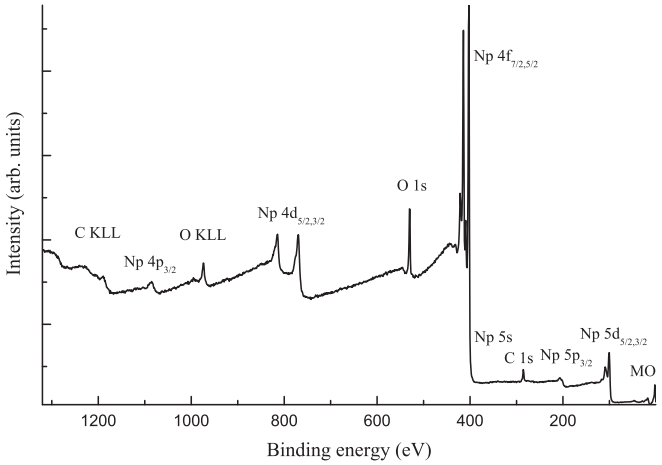

FIG. 1. Survey XPS from NpO_2.

the measurement error. The XPS studies of the Ar^+-cleaned samples after spending 1 d and more in the air indicated only the growth of the C 1*s* and the O 1*s* intensity due to oxygen- and carbon-containing surface contamination (agrees with Refs. 2, 5, and 8).

The powder NpO_2 sample did not contain more than ∼0.1 weight% of any metal impurities, since its survey XPS did not indicate any foreign peaks (Fig. 1). This BE range shows the O KLL and the C KLL Auger peaks from oxygen and carbon, respectively, as well as the C 1*s* peak from hydrocarbons on the sample surface. The surface hydrocarbon-related C 1*s* XPS was observed as a low intense $\Gamma(\text{C } 1s) = 1.3$ eV wide peak at $E_b(\text{C } 1s) = 285.0$ eV. As it was mentioned above, the valence XPS structure of NpO_2 in the BE range 0–∼35 eV reflects the MO structure. The contributions from other mechanisms of the XPS structure formation has to be taken into account also; therefore, the core electron XPS structure was analyzed.

A. Core-electron XPS structure of NpO_2

The O 1*s* XPS of NpO_2 was observed as a single peak at $E_b(\text{O } 1s) = 529.7$ eV and FWHM $\Gamma(\text{O } 1s) = 1.0$ eV (Table I), with a shoulder at $E_b(\text{O } 1s) = 531.2$ eV at the higher BE side from the basic peak attributed to hydroxyl groups and another shoulder at $E_b(\text{O } 1s) = 532.3$ eV attributed to absorbed water. The peak intensity ratio yielded 89% of NpO_2, 8% of OH^-, and 3% of H_2O (Fig. 2). The O 2*p* and the O 2*s* intensities from the OH^- and H_2O impurities do not increase too much the errors in the valence XPS decomposition since the O 2*s*,2*p* photoemission cross-section is significantly lower than the O 1*s* cross-section (Table I).

The Np 4*f* XPS from NpO_2 at the highest probability shows the many-body perturbation-related structure attributable to an extra electronic transition within the filled and the vacant valence levels during the Np 4*f* photoemission. It appears as shake-up satellites, whose parameters reflect the MO structure. As a result, the Np 4*f* XPS consists of the spin-orbit split doublet with $\Delta E_{sl}(\text{Np } 4f) = 11.7$ eV, and the shake-up satellites at the higher BE side with $\Delta E_{\text{sat}} = 6.9$ eV (Fig. 3). The satellite intensity ($I_{\text{sat}} = I_s/I_o$) calculated as the ratio of the XPS satellite area (I_s) to the basic peak area (I_o) was 18%. These satellites can serve as "fingerprints" for Np oxidation

TABLE I. Electron BEs E_b (eV) and photoionization cross-sections σ[a] at 1486.6 eV.

Np *nlj* O *nlj*	NpO_2	NpO_2[b]	Np_{met}[c]	Np_{theor}[d]	σ
Np 5*f*	1.7 (1.3)		0.3	0.3	24.6
Np 6$p_{3/2}$	17.2 (3.1)	17.5		17.5	5.33
Np 6$p_{1/2}$	29.0 (2.8)	29.3		29.1	1.81
Np 6*s*	46.7 (5.5)			50.1	2.34
Np 5$d_{5/2}$	100.4 (4.1)	100.9		100.0	49.3
Np 5$d_{3/2}$	∼108.9 (9.5)?			113.3	33.5
Np 5$p_{3/2}$	201.5				
	206.0	206.3		213.7	31.4
Np 5$p_{1/2}$	273 (10)			273.6	9.22
Np 5*s*	∼337			342.2	10.2
	∼346				
Np 4$f_{7/2}$	402.6 (1.6)	402.5	400.1	401.3	396
Np 4$f_{5/2}$	414.3 (1.6)	414.3	411.8	413.8	310
Np 4$d_{5/2}$	769.5 (5.0)	771.2		772.5	238
Np 4$d_{3/2}$	814.5 (5.0)	816.1		817.8	156
Np 4$p_{3/2}$	1084.8 (13.6)			1089.5	108
O 2*p*	∼3.9 (2.9)				0.27
	∼6.4 (1.8)				
O 2*s*	∼21.6	23.8			1.91
O 1*s*	529.7 (1.0)	529.7			40

[a]Photoionization cross-section σ_i (kiloBarn per atom) from Ref. 46.
[b]Values given relative to the C 1*s* BE $E_b(\text{C } 1s) = 285.0$ eV from Ref. 2.
[c]Values given for maxima, Np 4$f_{7/2}$ BE difference for NpO_2 and Np_{met} is 3.9 eV, Np 5$f_{7/2}$ BE difference for NpO_2 and Np_{met} is 2.7 eV.[5,8]
[d]Calculation data from Ref. 39, values given relative to the Np 5*f* peak from metallic Np.

state determination. In particular, this Np 4*f* structure and the satellites structure are typical for the Np(IV) oxidation state.[2,5,8,23] This spectrum also shows the satellites with $\Delta E_{\text{sat}^*} = 17.2$ eV at the higher BE side from the basic peaks. These satellites have two peaks separated by 2.2 eV. The satellite with $\Delta E_{\text{sat}^*} = 17.2$ eV from the Np 4$f_{7/2}$ peak is superimposed with the one with $\Delta E_{\text{sat}} = 6.9$ eV from the

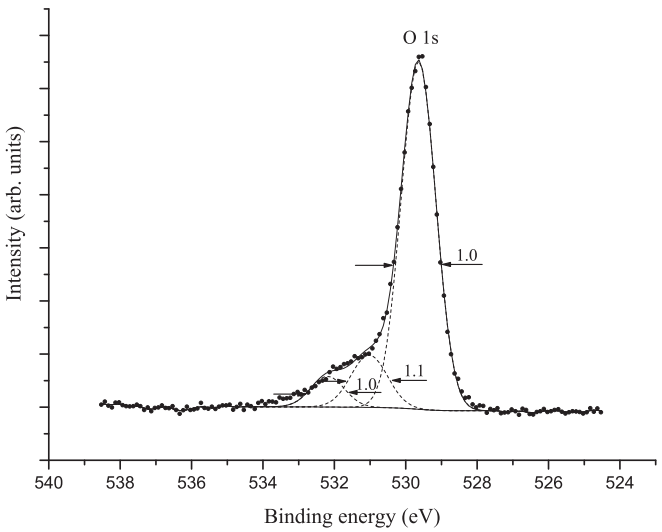

FIG. 2. O 1*s* XPS from NpO_2.

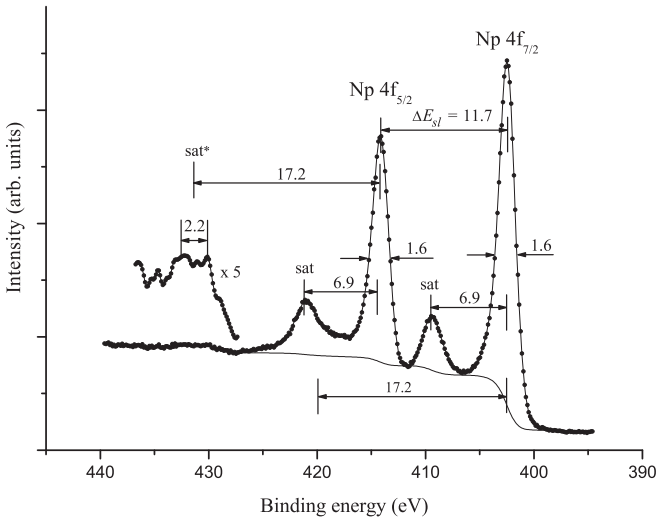

FIG. 3. Np 4*f* XPS from NpO_2.

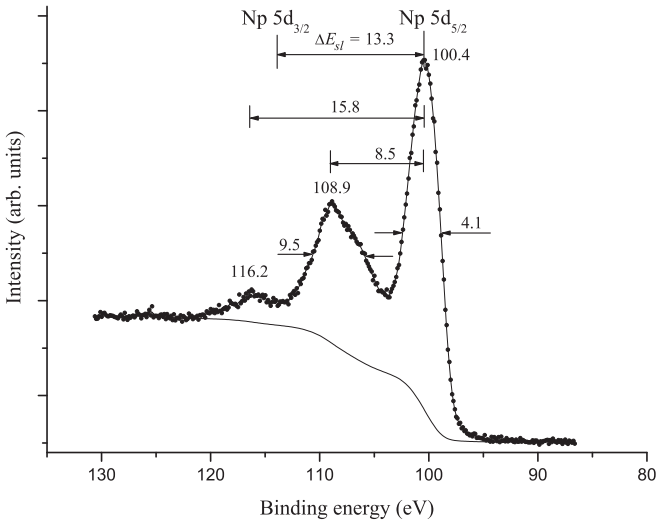

FIG. 5. Np 5*d* XPS from NpO_2.

Np $4f_{5/2}$ peak, which increases the intensity of the lower BE satellite. For the first half of the lanthanide compounds row, the shake-up satellites appear in the core-level XPS, and their intensity drops as the BE of the level decreases.[22] Such a satellite intensity drop was also observed in the PuO_2 XPS.[26] Therefore, the same satellites are expected in the other core-level XPS from NpO_2. Indeed, the Np $4d_{5/2}$ XPS [E_b(Np $4d_{5/2}$) = 769.5 eV and Γ(Np $4d_{5/2}$) = 5.0 eV] exhibits shake-up satellites at ΔE_{sat}(Np $4d_{5/2}$) = 6.9 eV at the higher BE side from the basic peak. Its intensity was I_{sat} = 34% (Fig. 4). Such satellites can contribute to the other XPS structures like Np $4p_{3/2}$, Np 5*s*, Np 5*p*, Np 5*d*, and Np 6*s* (see, e.g. Figs. 5–9). However, it is difficult to separate the shake-up satellite-related structure, since the multiplet splitting and the dynamic effect are more probable in these spectra.[23] Despite this, the extrapolation of the Np 4*d* and the Np 4*f* shake-up satellite intensity as the BE tends to zero predicts the shake-up satellite intensity in the valence band XPS not to exceed 10%, which agrees with the corresponding results for PuO_2.[26]

The multiplet splitting caused by the presence of the uncoupled Ln 4*f* electrons in lanthanide compounds results in the Ln 4*d* XPS structure.[22] Therefore, the multiplet splitting was expected to show up with the higher probability in the Np 5*d* XPS.[2,23] Indeed, the Np 5*d* spectrum instead of a spin-orbit split doublet [ΔE_{sl}(Np $5d$)$_{theor.}$ = 13.3 eV (Ref. 39)] exhibits a complicated structure with the Np $5d_{5/2}$ maximum at 100.4 eV (Fig. 5). This structure can be explained by the multiplet splitting superimposed with the shake-up satellites. Therefore, it is difficult to separate the satellite-related structure and to determine the satellite intensities. The multiplet splitting is very likely to show up in the Ln 4*s* XPS from lanthanide oxides.[22] In the Ln 5*s* XPS, it is about twice lower probable. This interaction results in the two components in the Ln *ns* XPS. Therefore, the Np 5*s* and the Np 6*s* XPS are expected to exhibit the multiplet splitting (Figs. 6 and 7).

To evaluate the multiplet splitting in the Np 5*s* and the Np 6*s* XPS, one can use the simplified expression for an ion with uncoupled electrons.[40] An ion with an incompletely filled valence shell electronic configuration nl^v, for example, the

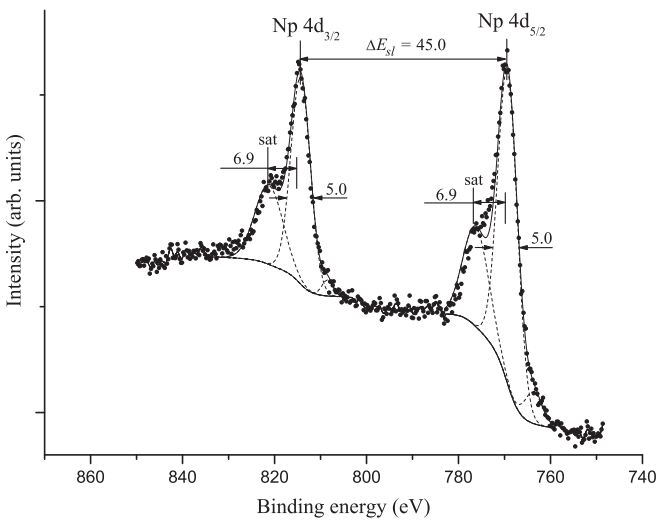

FIG. 4. Np 4*d* XPS from NpO_2.

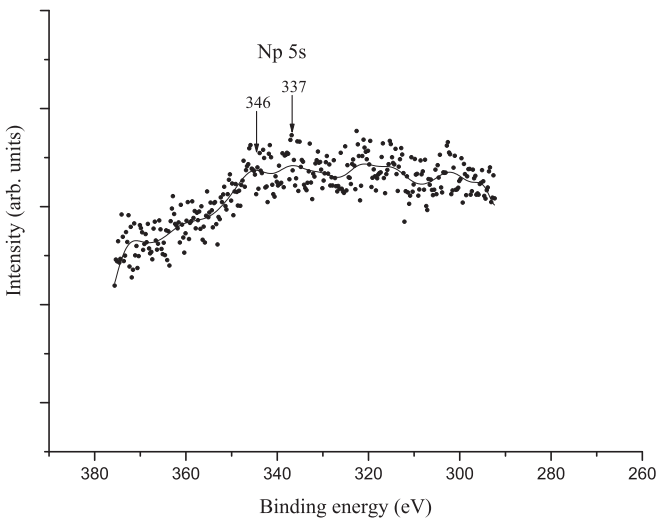

FIG. 6. Np 5*s* XPS region from NpO_2.

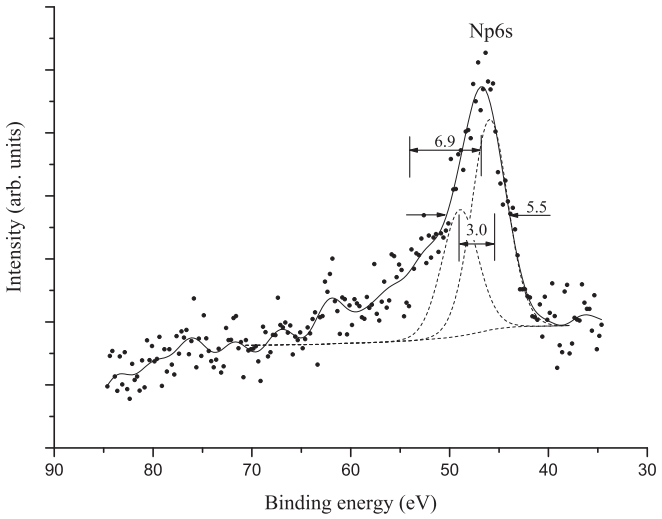

FIG. 7. Np 6*s* XPS from NpO_2.

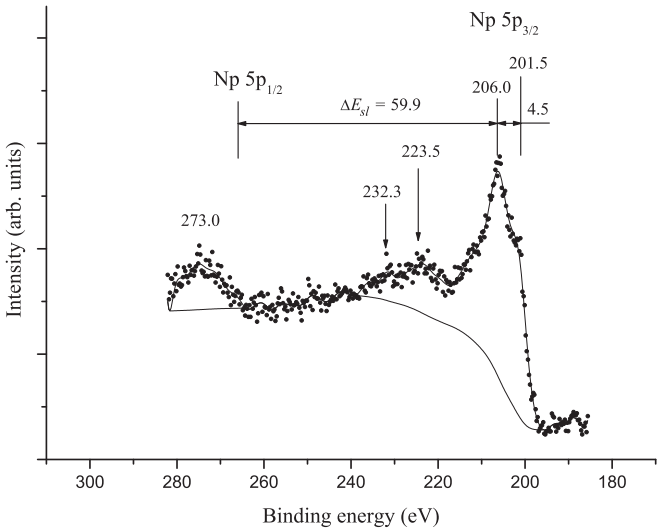

FIG. 8. Np 5*p* XPS from NpO_2.

Np $5f^3$ for Np(IV), has two final states after the electron photoemission from the core $n's$ shell. They are formed from the configurations $n's$ and nl^v. The energy difference ΔE_{ms} between these two states in this approximation is[40]

$$\Delta E_{ms} = [(2S+1)/(2l+1)]G^l(n's,nl), \quad (2)$$

where S is the initial spin attributable to the coupling of the nl electrons (n and l are the principal and orbital quantum numbers), and $G^l(n's,nl)$ is the corresponding atomic exchange Slater integral, e.g., for the Np(IV) ion. From Eq. (2), it follows that ΔE_{ms} is proportional to the multiplicity $(2S+1)$ or to the number of the uncoupled electrons in the ion. The intensity ratio of the doublet components I_1/I_2 has to be equal to the ratio of the multiplicities of the final states:

$$I_1/I_2 = (S+1)/S. \quad (3)$$

In this approximation, for the Np(IV) ion with the electronic configuration Np $5f^3$ and the Slater integral $G^3(5s,5f) = 7.81$ eV, the Np 5*s* multiplet splitting is ΔE_{ms}(Np 5*s*) = 4.46 eV and the Np 5*s* doublet intensity ratio is 5:3, while for $G^3(6s,5f) = 5.26$ eV, the splitting is ΔE_{ms}(Np 6*s*) = 3.0 eV and the intensity ratio in the Np 6*s* doublet is also 5:3.

The Np 6*s* XPS structure can be considered to contain a ΔE_{ms}(Np 6*s*) = 3.0 eV split doublet with the intensity ratio of 5:3 (Fig. 7). In reality, this XPS structure is more complicated, as well as the Np 5*s* structure (Fig. 6). It can be explained by the dynamic effect-related structure. This process was studied earlier[41] for the Th 5*p* XPS structure from metallic Th and Th and U compounds.[42,43] Reference 42 presents the interaction integrals of different configurations for thorium. These data show that the dynamic effect has to manifest with the highest probability in the An 5*p* and An 5*s* XPS; it is also highly probable in the An 6*s* XPS.

The dynamic effect is related to the gigantic Coster-Kronig transitions, e.g. the one observed in the Np 5*p* XPS (Fig. 8). It shows up as the peaks in the Np $5p_{3/2}$ doublet component at 201.5, 206.0, 212.0, 223.5, and 232.3 eV and as the peaks in the Np $5p_{1/2}$ doublet component at 273.0 eV. The Np 5*p* electron photoemission results in the complex final Np ion state determined by the interaction of the ground final state Np $5p^5 5d^{10} 5f^n$ and the excited two-hole final state Np $5p^6 5d^8 5f^{n+1}$ close by energy. This suggestion is based on the correlation of the Np 5*p* [E_b(Np $5p_{3/2}$) ~ 206.0 eV] and the Np 5*d* [E_b(Np $5d_{5/2}$) = 100.4 eV] BEs, which is close to the condition: E_b(Np $5p_{3/2}$) ≈ 2 × E_b(Np $5d_{5/2}$) (Table I). As a result, the probability of the extra final state Np $5p^6 5d^8 5f^{n+1}$ grows.

The Np 5*s* XPS is expected around E_b(Np 5*s*)$_{theor}$ ~ 342.2 eV, as it follows from the calculations[39] (Table I). For metallic Pu, the Pu 5*s* XPS was observed in the range ~35 eV and contained two structured peaks at 353.1 and 365.1 eV (Γ ~ 10 eV).[44] This structure can be attributed to both the multiplet splitting and the dynamic effect.[23] In this paper, it did not allow a reliable measurement of the Np 5*s* XPS. In this BE range, the peaks at 337 and 346 eV were observed (Table I, Fig. 6). One of the reasons for this structure is the dynamic effect resulting in the interaction of the configurations of the final states Np $5s^1 5p^6 5d^{10} 5f^n$ and Np $5s^2 5p^5 5d^9 5f^{n+1}$. Indeed, for the Np 5*s*, Np 5*p*, and Np 5*d* BEs (Table I), the condition E_b(Np 5*s*) ≈ E_b(Np 5*p*) + E_b(Np $5d_{3/2}$) is met, which does not contradict the possibility of formation of these configurations. The BEs E_b(Np $4p_{3/2}$) = 1084.8 eV, E_b(Np $4d_{5/2}$) = 769.5 eV, and E_b(Np 5*s*) ~ 342.2 eV approximately meet the condition E_b(Np $4p_{3/2}$) ~ E_b(Np $4d_{5/2}$) + E_b(Np 5*s*). Therefore, one can attribute the Np $4p_{3/2}$ XPS structure of NpO_2 to the dynamic effect with the interaction of the final states Np $4p^5 4d^{10} 5s^2 5f^n$ and Np $4p^6 4d^9 5s^1 5f^{n+1}$. Also, the shake-up satellite 6.9 eV away from the basic peak can superimpose on this structure (Fig. 9).

The Np 6*s* XPS exhibits a widened [Γ(Np 6*s*) = 5.5 eV] structured line at 46.7 eV (Fig. 7). One of the reasons for such structure, as it was already remarked, is the multiplet splitting. Another reason for this structure can be the dynamic effect resulting in the interaction of the configurations of the Np(IV) ion final states like Np $6s^1 6p^6 6d^0 5f^n$ and Np $6s^2 6p^4 6d^1 5f^n$. Indeed, for the BEs E_b(Np 6*s*) = 46.7 eV, E_b(Np $6p_{3/2}$) = 17.2 eV, and E_b(Np $6p_{1/2}$) = 29.0 eV (Table I), the condition E_b(Np 6*s*) ~ 2 × E_b(Np 6*p*) is met. Indeed, alone with the multiplet-splitting-associated structure, the extra complex

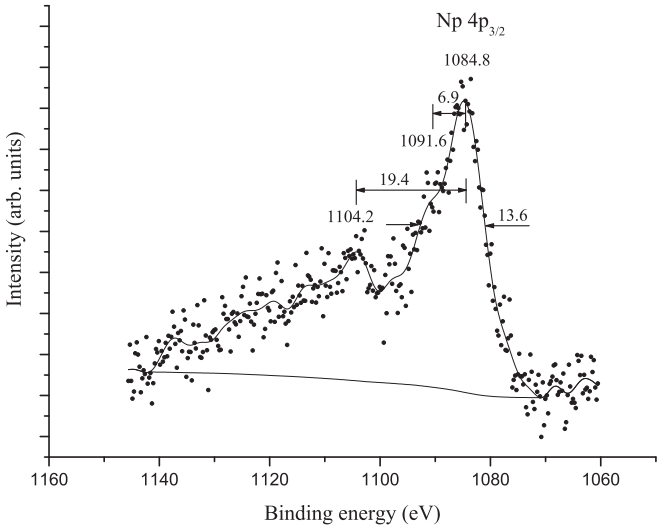

FIG. 9. Np $4p_{3/2}$ XPS from NpO_2.

dynamic effect- and shake-up satellite-related structure was observed (Fig. 7). Therefore, the considered XPS parameters cannot yield a conclusion on the possible participation of the Np 6*s* electrons in the MO formation.

The measured Np $4f$ BEs and structure parameters agree with the corresponding data obtained earlier for NpO_2.[2] Since the XPS structure in the An $6p$ BE range ongoing from ThO_2 to NpO_2 does not differ significantly in shape,[2,23] while the number of the quasi-atomic An $5f$ electrons grows from 0 to 3, one can suggest that the multiplet splitting does not play a primary role in the valence XPS structure formation in the BE range ∼15–∼35 eV. The dynamic effect-related structure is also low probability in this BE range because of the atomic states, but the quasi-atomic Np $5f$ structures are absent in the valence band. As a result, a suggestion can be drawn that the valence XPS structure in a high degree can be attributed to the MO formation, except for the peak at 8.8 eV (Fig. 10). The peak at 8.8 eV is 7.1 eV away from the peak of the localized Np $5f$ electrons [E_b(Np $5f$) = 1.7 eV] and, therefore, can be attributed to the many-body perturbation. The obtained data also allow a conclusion that the studied sample by its stoichiometry is close to NpO_2. One of the general reasons for the structure formation in the BE range from 0 to ∼35 eV for NpO_2, as it was already remarked, is the OVMO and IVMO formation. For the interpretation of the MO-related valence band XPS structure, the results of electronic structure calculations of the finite cluster in NpO_2 were used.

B. Electronic structure of the NpO_8 cluster

Neptunium atom ground state configuration $^6L_{5-1/2}$ can be presented as [Rn]$6s^2 6p^6 5f\ ^4 6d^1 7s^2 7p^0$, where [Rn] is radon electronic configuration, and the other electronic shells are valence and can participate in the MO formation.[21,23] For the illustration of general structure of the main molecular states, we use the results of the RDV calculations for the NpO_8 cluster, which models only the nearest Np environment in NpO_2. The characteristics of all vacant and occupied MOs in the energy region from 0 to 50 eV obtained for this cluster are given in Table II.

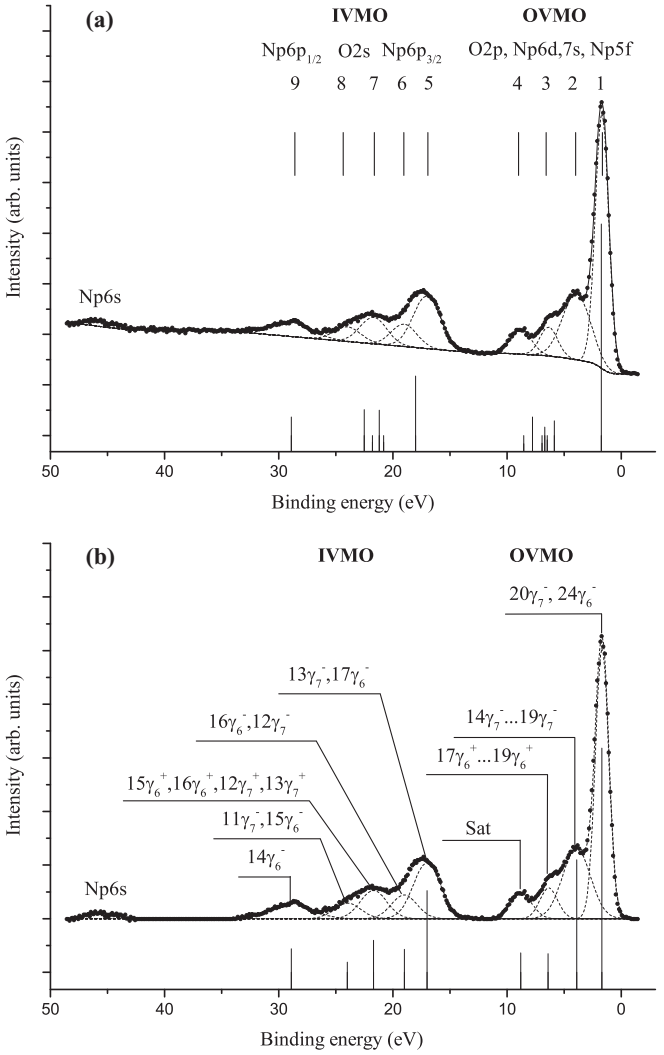

FIG. 10. Valence band XPS from NpO_2: (a) spectrum with the secondarily scattered electron background. The dashed lines show the division of the spectrum into separate components, vertical bars show the calculated (RDV) spectrum; (b) spectrum with subtracted background. The dashed lines show the division of the spectrum into separate components, vertical bars show the correct expected spectrum.

The RDV method is based on the MOs as linear combinations of AOs (LCAO) approach, which allows one to use both atomic and molecular terms for the chemical bond description. Indeed, the OVMOs and the IVMOs are formed during the chemical bond formation and the overlap of AOs of the neighboring neptunium and oxygen atoms. These MOs in addition to the Np 6*s*, $6p$, $5f$, $6d$, $7s$, and the O $2s$, $2p$ AOs also contain the Np $7p$ states, which are vacant in the isolated neptunium atom. In contrast to the results of the NR-calculations of NpO_2,[10] which show a significant participation of the Np 6*s* AOs in the MO formation, the results of the relativistic calculations show that the Np 6*s* AOs participate insignificantly in the MO formation (Table II). However, the Np $7s$ and the Np $7p$ AOs participate significantly in the MO formation. While the contributions from the Np $5f$ AOs were obtained mostly in the OVMO bands, the Np $6p$ and $6d$ AOs participate in both the OVMO and the IVMO states.

TABLE II. Composition and energies E_0[a] (eV) for the NpO_8 cluster (RDV) and photoionization cross-sections σ_i[b].

			MO composition												
			Np										O		
Mo		$-E_0$, eV	$6s$	$6p_{1/2}$	$6p_{3/2}$	$6d_{3/2}$	$6d_{5/2}$	$7s$	$5f_{5/2}$	$5f_{7/2}$	$7p_{1/2}$	$7p_{3/2}$	$2s$	$2p_{1/2}$	$2p_{3/2}$
			σ_i 1.16	0.90	1.32	0.62	0.56	0.12	4.12	3.86	0.06	0.08	0.96	0.07	0.07
OVMO	22 γ_7^+	−7.76					0.83						0.05	0.09	0.03
	21 γ_7^+	−7.40				0.43	0.40						0.05	0.03	0.09
	25 γ_6^+	−7.40				0.43	0.39						0.05	0.02	0.11
	24 γ_6^+	−5.30						0.88					0.06	0.02	0.04
	28 γ_6^-	−5.30								0.02	0.90		0.04	0.02	0.02
	27 γ_6^-	−3.74			0.01							0.92	0.03		0.04
	24 γ_7^-	−3.69										0.93	0.03		0.04
	23 γ_6^+	−3.65				0.40	0.45							0.04	0.11
	20 γ_7^+	−3.65				0.40	0.45							0.04	0.11
	23 γ_7^-	−1.66							0.10	0.76			0.01	0.07	0.06
	26 γ_6^-	−0.93							0.01	0.93				0.02	0.04
	22 γ_7^-	−0.93								0.93				0.02	0.05
	25 γ_6^-	−0.92								0.93	0.01			0.05	0.01
	21 γ_7^-	−0.14							0.80	0.14				0.01	0.05
	24 γ_6^-[c]	0.00							0.91	0.01					0.08
	20 γ_7^-	0.00							0.92	0.01					0.07
	19 γ_7^-	4.11												0.30	0.70
	23 γ_6^-	4.11												0.30	0.70
	22 γ_6^-	4.22			0.05				0.05	0.02				0.18	0.70
	18 γ_7^-	4.22			0.05				0.05	0.02				0.30	0.58
	19 γ_7^+	4.32												0.15	0.85
	22 γ_6^+	4.32												0.15	0.85
	21 γ_6^+	4.33												0.66	0.34
	18 γ_7^+	4.60					0.01							0.06	0.93
	17 γ_7^+	4.63				0.01								0.48	0.51
	20 γ_6^+	4.64				0.01								0.48	0.51
	21 γ_6^-	4.74								0.06	0.01			0.82	0.11
	17 γ_7^-	4.95							0.07	0.07				0.29	0.57
	16 γ_7^-	5.18			0.01				0.01	0.01		0.04		0.19	0.74
	20 γ_6^-	5.19			0.01				0.01	0.01		0.04		0.10	0.83
	19 γ_6^-	5.52		0.01							0.04		0.01	0.31	0.63
	15 γ_7^-	6.03							0.02	0.03				0.17	0.78
	18 γ_6^-	6.03							0.02	0.03				0.17	0.78
	14 γ_7^-	6.04							0.03	0.02				0.63	0.32
	19 γ_6^+	6.07						0.05					0.01	0.32	0.62
	16 γ_7^+	6.12				0.01	0.10						0.01	0.57	0.31
	18 γ_6^+	6.14				0.07	0.05						0.01	0.03	0.84
	15 γ_7^+	6.15				0.07	0.05						0.01	0.30	0.57
	14 γ_7^+	6.80				0.06	0.08							0.28	0.58
	17 γ_6^+	6.82				0.06	0.08							0.28	0.58
IVMO	17 γ_6^-	16.26			0.67							0.02	0.25	0.02	0.04
	13 γ_7^-	16.26			0.66							0.01	0.26	0.03	0.04
	12 γ_7^-	19.09											0.98		0.02
	16 γ_6^-	19.37		0.03							0.04		0.93		
	13 γ_7^+	19.51					0.06						0.94		
	12 γ_7^+	19.52				0.02	0.03						0.95		
	16 γ_6^+	19.52				0.03	0.02						0.95		
	15 γ_6^+	20.04	0.01					0.07					0.92		
	15 γ_6^-	20.74			0.27							0.02	0.70		0.01
	11 γ_7^-	20.74			0.27							0.02	0.69	0.01	0.01
	14 γ_6^-	27.15		0.96									0.03		0.01
	14 γ_6^+	45.37	0.99										0.01		

[a]Levels shifted by 15.16 eV toward the positive values (upward).

[b]Photoionization cross-sections σ_i (kiloBarn per electron) for O from Ref. 46 and for Np from Ref. 47.

[c]Highest occupied MO (HOMO; 1 electron), occupation number for all the orbitals is 2.

Especially significant mixing of the Np $6p_{3/2}$ and O $2s$ AOs was observed for the $17\gamma_6^-$, $13\gamma_7^-$ (5) and $15\gamma_6^-$, $11\gamma_7^-$ (8) IVMOs (Table II). The mixing of the Np $6p_{1/2}$ and the O $2s$ AOs for the $16\gamma_6^-$ (6) and $14\gamma_6^-$ (9) IVMOs takes place to a lesser extent than in the corresponding orbitals in ThO_2 (Ref. 24) and UO_2.[25] This result can be explained by the increase of the spin-orbit splitting ΔE_{sl}(An $6p$) and by the increase of the An $6p_{1/2}$ BE with respect to that of the O $2s$ AOs as the atomic number Z grows in the actinide row. These results allow an interpretation of the valence XPS structure of NpO_2.

C. Valence XPS structure of NpO_2

The XPS from NpO_2 in the BE range 0–∼35 eV consists of a number of structured widened lines (Fig. 10). As it was already stated in the present paper, in this BE range, the many-body effects and the multiplet splitting can also show up. These effects more likely can show up in the XPS of the quasi-atomic Np $5f$ electrons participating weakly in the chemical bond formation.[2,23] However, it was found that, in particular, in actinide oxides, electrons from this BE range participate in the MO formation that results in the XPS structure.[21,23–26] For example, for NpO_2 the O $1s$ FWHM ($E_b = 529.7$ eV) is $\Gamma = 1.0$ eV, while the corresponding O $2s$ peak ($E_b \sim 21.6$ eV) is ∼4 eV wide and structured. It contradicts the Heisenberg uncertainty ratio $\Delta E \Delta\tau \approx h/2\pi$, where ΔE is the natural width of a level from which an electron was extracted, $\Delta\tau$ is the hole lifetime, and h is the Planck constant. Since the hole lifetime ($\Delta\tau$) grows as the absolute level energy decreases, the lower BE XPS peaks are expected to be narrower. Indeed, since the hole lifetime ($\Delta\tau$) grows as the absolute level energy decreases, the atomic spectral peaks are expected to narrow as the BE decreases. Therefore, the fact that the valence peaks are wider than the corresponding core peaks proves that this peak is not atomic and must be attributed to the IVMO formation in NpO_2.

The XPS from NpO_2 in the BE range 0–∼35 eV can be conditionally subdivided into two ranges (Fig. 10). The first range 0–∼15 eV exhibits the OVMO-related structure. These OVMOs are formed mostly from the Np $5f$, $6d$, $7s$, $7p$, and the O $2p$ AOs of the neighboring atoms, while the peak at 1.7 eV is related to the quasi-atomic Np $5f$ electrons. The multiplet splitting is most likely to result in the widening of this peak,[2,24] and the many-body perturbation is expected to manifest as a shake-up satellite on the higher-BE side from this peak at ∼6.9 eV. This satellite was observed in the XPS at 8.8 (Fig. 10). The second range ∼15–∼35 eV exhibits the IVMO-related structure. These IVMOs appear mostly due to the strong interaction of the completely filled Np $6p$ and O $2s$ AOs. The OVMO XPS structure has its typical features and can be subdivided into four components (1–4). The IVMO range exhibits explicit peaks and can be subdivided into five components (5–9; Fig. 10). Despite the formalism of such a division, it allows qualitative and quantitative comparison of the XPS parameters with the relativistic calculation results for the NpO_8 cluster.

Results of these calculations are given in Table II. Since photoemission results are given for an excited state of an atom with a hole on a certain shell, the calculations must be done for transition states for a stricter comparison of the theoretical and experimental BEs.[45] However, the valence electron BEs calculated for transition states are known to differ from the corresponding values for the ground state by a constant shift. Therefore, this paper gives the calculated BEs (Table II) shifted by 1.74 eV (Table III). Taking into account the MO compositions (Table II) and the photoionization cross-sections,[46,47] the theoretical intensities of several XPS ranges were determined (Table III). Comparing the experimental XPS to the theoretical data, one should keep in mind that the XPS from neptunium dioxide reflects the band structure and consists of bands widened due to the solid-state effects. Despite this approximation, a satisfactory qualitative agreement between the theoretical and the experimental data was obtained [Fig. 10(a)].

Indeed, the corresponding theoretical and experimental FWHMs and the relative intensities of the inner and outer valence bands are comparable [Table III, Fig. 10(a)]. A satisfactory agreement between the experimental and calculated BEs of some MOs was also reached (Table III). The worst discrepancy was observed for the middle IVMO XPS ($12\gamma_7^-$–$15\gamma_6^+$). As mentioned above, the NR X_α-DVM (Ref. 10) results allowed only qualitative interpretation of the low BE XPS of NpO_2. The present relativistic calculations practically allow a quantitative identification of the valence XPS of NpO_2 in the whole BE range of 0–∼35 eV [Table III, Fig. 10(b)]. The expected correct spectrum obtained on the basis of the calculations and the experimental data is given in Table III and drawn under the XPS as vertical bars [Fig. 10(b)]. These data promote the RDV method and underlie the quantitative MO scheme for understanding the nature of interatomic bonding in NpO_2.

Thus, the outer valence band intensity is formed mostly from the outer valence Np $5f$, $6d$, $7s$, $7p$, and O $2p$ AOs, and to a lesser extent from the inner valence Np $6p$ and O $2s$ AOs. The Np $5f$ electrons contribute significantly to the OVMO intensity (Tables II and III). Because the Np $5f$ photoemission cross-section is high (Tables I and III), the Np $5f$ electrons contribute significantly to the OVMO XPS intensity if they do not lose the f nature. For example, the Np $5f$ electrons can be promoted to the Np $6d$ level first and then participate in the chemical bond formation. They also can participate directly in the formation of the interatomic bond without losing the f nature. The electronic structure calculations for NpO_2 yielded that the Np $5f$ electrons participate directly in the chemical bond formation (Table II). In the ionic approximation for neptunium electronic configuration Np $6p^6 5f^4 6d^1 7s^2$ in NpO_2, the calculated OVMO/IVMO intensity ratio was found to be 1.63[23,48] which agrees with the corresponding theoretical value 1.63 and the experimental value 1.72 (see Table III) within the measurement error of ±10%. This intensity ratio is an important characteristic of the NpO_2 electronic structure. These results yield a conclusion that the Np $5f$ electrons participate directly in the chemical bond formation in NpO_2 partially losing the f nature. These electronic states are located closer to the middle and the top of the outer valence band (Tables II and III); the Np $6d$ electronic states are located at the bottom of the outer valence band. This agrees with the theoretical and the experimental data for ThO_2,[24] UO_2,[25] and PuO_2.[26]

TABLE III. Valence XPS parameters for NpO_2 and for the NpO_8 cluster (RDV), and the Np $6p$ and Np $5f$ electronic state density ρ_i (e^-).

MO		$-E$[a], eV	XPS Energy[b], eV	XPS Intensity, %		Np $6p$,$5f$ electronic state density ρ_i (e^-), e^- (electrons)			
			Experiment	Theory	Experiment	$5f_{5/2}$	$5f_{7/2}$	$6p_{1/2}$	$6p_{3/2}$
OVMO	24 γ_6^- [c]	1.74	1.7 (1.4)	13.4	34.4	0.91	0.01		
	20 γ_7^-	1.74		27.3		1.84	0.02		
	19 γ_7^-	5.85		0.1					
	23 γ_6^-	5.85		0.1					
	22 γ_6^-	5.86		2.5		0.10	0.04		0.10
	18 γ_7^-	5.86		2.5		0.10	0.04		0.10
	19 γ_7^+	6.06		0.1					
	22 γ_6^+	6.06		0.1					
	21 γ_6^+	6.07		0.1					
	18 γ_7^+	6.34		0.2					
	17 γ_7^+	6.37		0.2					
	20 γ_6^+	6.38		0.2					
	21 γ_6^-	6.48		1.5			0.12		
	17 γ_7^-	6.69	3.9(2.9)	4.4	18.5	0.14	0.14		
	16 γ_7^-	6.92		0.7		0.02	0.02		0.02
	20 γ_6^-	6.93		0.8		0.02	0.02		0.02
	19 γ_6^-	7.26		0.2				0.02	
	15 γ_7^-	7.77		1.4		0.04	0.06		
	18 γ_6^-	7.77		1.4		0.04	0.06		
	14 γ_7^-	7.78		1.4		0.06	0.04		
	19 γ_6^+	7.81		0.2					
	16 γ_7^+	7.86		0.6					
	18 γ_6^+	7.88	6.4(1.8)	0.6	5.1				
	15 γ_7^+	7.89		0.6					
	14 γ_7^+	8.54		0.7					
	17 γ_6^+	8.56		0.7					
	sat		8.8 (2.2)		5.2				
	ΣI_i[d]			62.0	63.2	3.27	0.57	0.02	0.24
IVMO	17 γ_6^-	18.00	17.0 (2.8)	6.8	14.1				1.34
	13 γ_7^-	18.00		6.7					1.32
	12 γ_7^-	20.83		1.7					
	16 γ_6^-	21.11	19.0(2.6)	1.8	5.7			0.06	
	13 γ_7^+	21.25		1.8					
	12 γ_7^+	21.26		2.0					
	16 γ_6^+	21.26	21.7(2.7)	1.8	7.0				
	15 γ_6^+	21.78		1.7					
	15 γ_6^-	22.48	24.0 (2.7)	3.8	3.9				0.54
	11 γ_7^-	22.48		3.7					0.54
	14 γ_6^-	28.89	28.9 (4.2)	6.2	5.8			1.92	
	ΣI_i[d]			38.0	36.8			1.98	3.74
	14 γ_6^+	47.11	46.7 (5.5)	~7.6	~4				

[a] Calculated energies (Table II) shifted by 1.74 eV toward the negative values (downward), so that the 24 γ_6^- MO energy is 1.7 eV.
[b] FWHM in eV given in parentheses.
[c] HOMO (1 electron), occupation number for all the orbitals is 2.
[d] The sum of peak intensities and Np $6p$, $5f$ electronic state densities.

The peak at 8.8 eV in the OVMO XPS of NpO_2 (Fig. 10) according to Ref. 2 was attributed to the multiplet splitting of the Np $5f^3$ Np(IV) spectrum. This peak cannot be attributed to the O $2p$ states as well because its intensity relative to the O $2s$ intensity is too high [see σ(O $2s$) and σ(O $2p$) in Table I, II].

Taking into account the quasi-atomic nature of the Np $5f^3$ electrons in NpO_2, as it was noted, one can expect shake-up satellites at $\Delta E_{sat} \approx 6.9$ eV similar to those in the Np $4f$ XPS (Fig. 3). Indeed, the considered peak was observed on the higher-BE side 7.1 eV away from the Np $5f$ peak at E_b(Np $5f$) = 1.7, which agrees with ΔE_{sat}(Np $4f$) = 6.9 eV. The intensity of this satellite relative to the Np $5f$ peak intensity is $I_{sat} = 15\%$ (see Table III).

In the IVMO XPS BE range, a satisfactory agreement was reached, e.g., for the $17\gamma_6^-$, $13\gamma_7^-$ (5), and $14\gamma_6^-$ (9)

MOs responsible for the width ΔE of this XPS band. The calculated $\Delta E_{\text{Theor}} = 10.89$ eV without taking into account the FWHMs is comparable with the experimental $\Delta E_{\text{exp}} = 11.9$ eV (Table III). It has to be noted that the theoretical (1.63) and experimental (1.72) OVMO/IVMO intensity ratios are comparable; that confirms correctness of the approximations used in the calculation (see Table III). The calculated and the experimental relative intensities of some individual IVMO peaks, except for the $17\gamma_6^-$ and $13\gamma_7^-$ (5) peaks, are in qualitative agreement.

Taking into account the experimental BE differences between the outer MOs and the core levels in NpO_2 and metallic Np,[5,8] as well as the relativistic calculation data for the NpO_8 cluster in the MO LCAO approximation, a quantitative MO scheme for NpO_2 (Fig. 11) was built. This scheme enables one to understand the real XPS structure and the chemical bond nature in NpO_2. In this approximation, one can pick out the antibonding $17\gamma_6^-$, $13\gamma_7^-$ (5), and $16\gamma_6^-$(6) and the corresponding bonding $15\gamma_6^-$, $11\gamma_7^-$ (8), and $14\gamma_6^-$ (9) IVMOs, as well as the quasi-atomic $12\gamma_7^-$, $13\gamma_7^+$, $12\gamma_7^+$, $16\gamma_6^+$, and $15\gamma_6^+$ (7) IVMOs attributed mostly to the O $2s$ electrons. The experimental data show that the O $2s$-related quasi-atomic IVMO BEs have to be close by magnitude. Indeed, the O $1s$ XPS of NpO_2 allows a suggestion that their chemical nonequivalence should not exceed 1 eV, since the O $1s$ peak was observed symmetric and 1.0 eV wide. The O $2s$ BE has to be about 21.6 eV, since the $\Delta E_O = 508.1$ eV and the

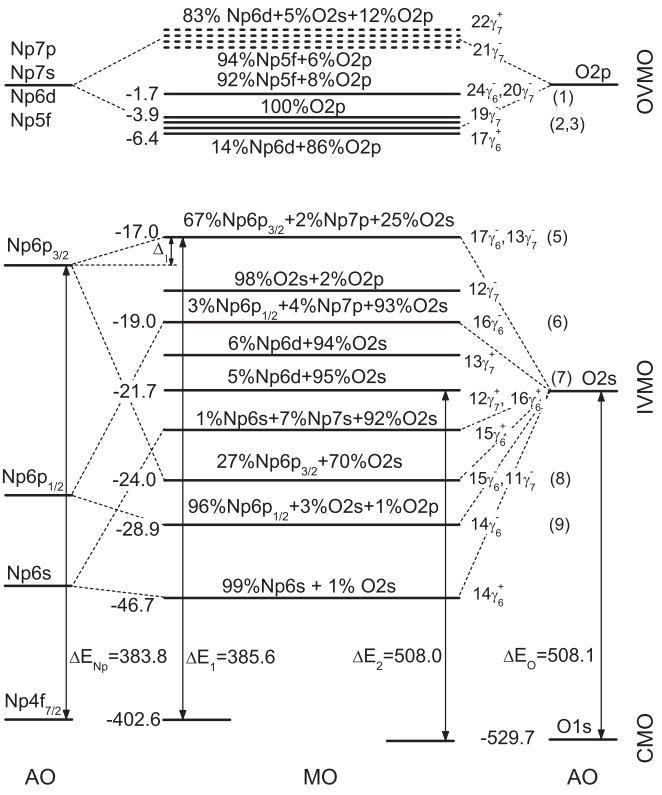

FIG. 11. MO scheme for the NpO_8 cluster built taking into account theoretical and experimental data. Chemical shifts are not indicated. Arrows show some measurable-level BE differences. Experimental BEs (eV) are given to the left. The energy scale is not kept.

O $1s$ BE in NpO_2 is $E_b = 529.7$ eV (Fig. 2). The theoretical results agree partially with these data. The IVMO FWHMs cannot yield a conclusion on the IVMO nature (bonding or antibonding); however, one can suggest that the admixture of 6% of the O $2p$ and 2% of the Pu $7p$ AOs in the $17\gamma_6^-$ and $13\gamma_7^-$ (5) IVMOs leads these orbitals to losing of their antibonding nature (Table II, Fig. 11, see also Ref. 21). Thus, the quantitative MO scheme for NpO_2 built on the basis of the experimental and the theoretical data allows one both to understand the nature of chemical bond formation in NpO_2 and to interpret the structures of other x-ray spectra of NpO_2 as it was shown for ThO_2,[24] UO_2,[25] and PuO_2.[26]

D. O KLL Auger spectrum structure of NpO_2

The MO scheme for NpO_2 (Fig. 11) was used to explain qualitatively the Auger O KLL spectral structure of NpO_2 (Fig. 12). For example, the O KLL Auger spectrum of Al_2O_3 with poorly formed IVMO is known to consists of three well-observable poorly structured ~9-eV-wide peaks reflecting the O $KL_{2\text{-}3}L_{2\text{-}3}$ (O $1s \leftarrow$ O $2p$), the O $KL_1L_{2\text{-}3}$ (O $1s \leftarrow$ O $2s$, $2p$), and the O KL_1L_1 (O $1s \leftarrow$ O $2s$) transitions.[49] The relative intensities of these Auger O KLL peaks are given as the Auger O KLL to the XPS O $1s$ intensity ratios. These relative intensities are important fundamental values. They allow a quantitative comparison of, for example, the O $2p$ partial density of states (DOS) on oxygen ions in various oxides.

The Auger $OKL_{2\text{-}3}L_{2\text{-}3}$ (O $1s \leftarrow$ O $2p$) ($\Gamma = 4.5$ eV) spectrum of NpO_2 reflects the filled O $2p$ DOS in NpO_2 (Fig. 12). The O $KL_{2\text{-}3}L_{2\text{-}3}$ FWHM is comparable with the FWHMs' sum of the XPS O $1s$ electron peak ($\Gamma = 1.0$ eV, Fig. 2) and the O $2p$ DOS peaks (2, 3) in NpO_2 ($\Gamma \sim 5$ eV, Fig. 10, Table III). This Auger line consists of three peaks (see Fig. 12). The energy differences between these peaks are in a satisfactory qualitative agreement with the corresponding energy differences between the three OVMO XPS peaks (see Fig. 10). From the intensity ratio of the Auger $OKL_{2\text{-}3}L_{2\text{-}3}$ peaks, it follows that the quasi-atomic $24\gamma_6^-$ and $20\gamma_7^-$ (1) OVMOs contain the O$2p$ states, which agrees with the calculation results (Table II). The O $KL_1L_{2\text{-}3}$ (O $1s \leftarrow$ O

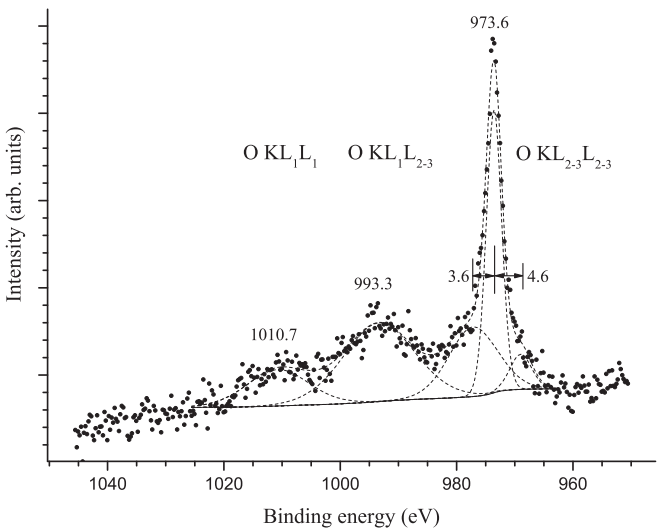

FIG. 12. Auger O KLL spectrum from NpO_2.

$2s, 2p$) peak reflects both the O $2p$ and the O $2s$ DOSs. This peak is complicated and difficult to explain. The O KL_1L_1 (O $1s \leftarrow$ O $2s$) peak reflecting mostly the DOS of the O $2s$ electrons participating in the IVMO formation in NpO_2 is highly structured. The FWHM of this peak $\Gamma \sim 13$ eV is comparable to that of the IVMO electrons in the XPS spectrum. It confirms the participation of the O $2s$ electrons in the IVMO formation (Figs. 10 and 12). These results agree with the O KLL Auger data for ThO_2,[24] UO_2,[25] and PuO_2.[26]

In conclusion, we would like to note that this paper studied the XPS structure of NpO_2 in the BE range of 0 to ~35 eV and established a correlation between this structure's (OVMO and IVMO related) parameters with the participation of the valence Np $6s, 6p, 5f, 6d, 7s, 7p$, and the O $2s, 2p$ electrons in the chemical bond of neptunium dioxide.

V. CONCLUSIONS

The XPS structure of NpO_2 was studied in the BE range 0–1250 eV. The correlation of the XPS structure parameters with the mechanisms of its formation were established. With the BE differences between the core and valence electronic levels and the relativistic calculation results of the electronic structure of the NpO_8 cluster in mind, a quantitative interpretation was done of the XPS structure of the OVMO (0 to ~15 eV BE) and the IVMO (~15 to ~35 eV BE) for neptunium dioxide NpO_2. The Np $5f$ (1.06 Np $5f$ e^-) electrons were theoretically shown and experimentally confirmed to participate directly in the chemical bond formation in NpO_2. The quasi-atomic Np $5f$ electrons (2.78 Np $5f$ e^-) were shown to be localized mostly at 1.7 eV. The Np $6p$ electrons, in addition to their effective (experimentally measurable) participation in the IVMO formation, were found to contribute noticeably (~0.3 Np $6p$ e^-) in the occupied part of the OVMO in NpO_2. The results of our investigation showed that the great role in the IVMO formation in NpO_2 was played by the Np $6p_{3/2}$ and the O $2s$ AOs of the neighboring neptunium and oxygen ions. The MO sequent order in the BE range of 0–~35 eV for NpO_2 was defined, and the corresponding MO composition was obtained in the cluster calculations. It allowed a fundamental quantitative MO scheme, which is important for understanding the nature of interatomic bonding in NpO_2 and for the interpretation of its other x-ray spectra.

ACKNOWLEDGMENTS

The work was supported by the RFBR Grant No.13-03-00214-a. We thank V. G. Yarzhemsky for the calculation of the Slater exchange integrals and for the discussion of the results. We also thank V. V. Kharitonova for help in the XPS data processing and representation. The authors declare no competing financial interests.

*Corresponding author: Teterin_YA@nrcki.ru

[1] K. T. Moor and G. van der Laan, Rev. Mod. Phys. **81**, 235 (2009).
[2] B.W. Veal, H. Diamond, and H. R. Hoekstra, Phys. Rev. B **15**, 2929 (1977).
[3] B.W. Veal, D. J. Lam, and H. Diamond, Physica B + C **86-88**, 1193 (1977).
[4] J. R. Naegele, J. Ghijsen, and L. Manes, Struct. Bonding **59-60**, 197 (1985).
[5] J. R. Naegele, L. E. Cox, and J. W. Ward, Inorg. Chim. Acta. **139**, 327 (1987).
[6] B. P. Pan and A. B. Campbell, Radiochim. Acta. **81**, 73 (1998).
[7] J. R. Naegele, J. Nucl. Mater. **166**, 59 (1989).
[8] A. Seibert, T. Gouder, and F. J. Huber, Nucl. Mater., **389**, 470 (2009).
[9] R. C. Albers, A. M. Boring, J. M. Wills, L. E. Cox, O. E. Eriksson, and N. E. Christensen, Phys. Rev. B **54**, 14405 (1996).
[10] V. A. Gubanov, A. Rosen, and D. E. Ellis, J. Phys. Chem. Solids. **40**, 17 (1979).
[11] I. D. Prodan, G. E. Scuseria, and R. L. Martin, Phys. Rev. B **76**, 033101 (2007).
[12] D. A. Andersson, J. Lezama, B. P. Uberuaga, C. Deo, and S. D. Conradson, Phys. Rev. B **79**, 024110 (2009).
[13] M.-T. Suzuki, N. Magnani, and P. M. Oppeneer, Phys. Rev. B **82**, 241103(R) (2010).
[14] L. Petit, A. Svane, Z. Szotek,W. M. Temmerman, and G. M. Stocks, Phys. Rev. B **81**, 045108 (2010).
[15] B.-T. Wang, H. Shi, W. Li, and P. Zhang, Phys. Rev. B **81**, 045119 (2010).
[16] Y. Yun, J. Rusz, M.-T. Suzuki, and P. M. Oppeneer, Phys. Rev. B **83**, 075109 (2011).
[17] X.-D. Wen, R. L. Martin, L. E. Roy, G. E. Scuseria, S. P. Pudin, E. R. Batista, T. M. McGleskey, B. L. Scott, E. Bauer, J. J. Joyce, and T. Durakiewicz, J. Chem. Phys. **137**, 154707 (2012).
[18] W. D. Zhou, C. Z. Dong, Q. M. Wang, X. L. Wang, L. A. Saber, Eur. Phys. J. D **66**, 260 (2012).
[19] Z. Rak, R. C. Ewing, and U. Becker, Surf. Sci. **608**, 180 (2013).
[20] Yu Yang and P. Zhang, J. Appl. Phys. **113**, 013501 (2013).
[21] Y. A. Teterin and S. G. Gagarin, Russ. Chem. Rev. **65**, 825 (1996).
[22] Y. A. Teterin and A. Y. Teterin, Russ. Chem. Rev. **71**, 347 (2002).
[23] Y. A. Teterin and A. Y. Teterin, Russ. Chem. Rev. **73**, 541 (2004).
[24] A. Y. Teterin, M. V. Ryzhkov, Y. A. Teterin, L. Vukcevic, V. A. Terekhov, K. I. Maslakov, and K. E. Ivanov, Radiochemistry **51**, 560 (2009).
[25] Yu. A. Teterin and A. Yu. Teterin, Radiochemistry **47**, 440 (2005).
[26] Yu. A. Teterin, K. I. Maslakov, A. Yu. Teterin, K. E. Ivanov, M. V. Ryzhkov, V. G. Petrov, D. A. Enina, and St. N. Kalmykov, Phys. Rev. B **87**, 245108 (2013).
[27] A. Yu. Teterin, M. V. Ryzhkov, Yu. A. Teterin, A. D. Panov, A. C. Nikitin, K. E. Ivanov, and I. O. Utkin, Radiochemistry **44**, 224 (2002).
[28] A. Y. Teterin, Y. A. Teterin, K. I. Maslakov, A. D. Panov, M. V. Ryzhkov, and L. Vukcevic, Phys. Rev. B **74**, 045101 (2006).
[29] I. O. Utkin, Yu. A. Teterin, V. A. Terekhov, M. V. Ryzhkov, A. Yu. Teterin, and L. Vukcevic, Nucl. Technol. Radiat. Protection **19**, 15 (2004).

[30]D. A. Shirley, Phys. Rev. B **5**, 4709 (1972).
[31]T. Gouder and L. Havela, Mikrochim. Acta **138**, 207 (2002).
[32]P. Morrall, P. Roussel, L. Jolly, A. Brevet, and F. Delaunay, J. Nucl. Mater. **385**, 15 (2009).
[33]G. H. Lander and M. H. Mueller, Phys. Rev. B **10**, 1994 (1974).
[34]A. Rosen and D. E. Ellis, J. Chem. Phys. **62**, 3039 (1975).
[35]D. E. Ellis and G. L. Goodman, Int. J. Quant. Chem. **25**, 185 (1984).
[36]O. Gunnarsson and B. I. Lundqvist, Phys. Rev. B **13**, 4274 (1976).
[37]P. Pyykko and H. Toivonen, Acta Acad. Aboensis, Ser. B: Math. Phys. **43**, 50 (1983)
[38]D. A. Varshalovish, A. N. Moskalev, and V. K. Khersonskii, *Quantum Theory of Angular Momentum* (World Scientific, Singapore, 1988).
[39]K. N. Huang, M. Aojogi, M. N. Chen, B. Graseman, and H. Mark, At. Data Nucl. Data Tables **18**, 243 (1976).
[40]J. H. Van Vleck, Phys. Rev. **45**, 405 (1934).
[41]T. K. Sham and G. Wendin, Phys. Rev. Lett. **44**, 817 (1980).
[42]G. T. Bancroft, T. K. Sham, and S. Larsson, Chem. Phys. Lett. **46**, 551 (1977).
[43]M. Boring, R. D. Cowan, and R. L. Martin, Phys. Rev. B **23**, 445 (1981).
[44]R. Baptist, D. Courteix, J. Chayrouse, and L. Heintz, J. Phys. F: Met. Phys. **12**, 2103 (1982).
[45]C. Slater and K. H. Johnson, Phys. Rev. B **5**, 844 (1972).
[46]J. H. Scofield, J. Electron Spectrosc. & Relat. Phenom. **8**, 129 (1976).
[47]V. G. Yarzhemsky, A. Y. Teterin, Y. A. Teterin, and M. B. Trzhaskovskaya, Nucl. Technol. Radiat. Protection **27**, 103 (2012).
[48]Y. A. Teterin, A. Y. Teterin, K. E. Ivanov, and I. O. Utkin, J. Nucl. Sci. Technol., Suppl. **3**, 140 (2002).
[49]Y. A. Teterin, K. E. Ivanov, A. Y. Teterin, A. M. Lebedev, I. O. Utkin, and L. Vukchevich, J. Electron Spectrosc. & Relat. Phenom. **101-103**, 401 (1999).